

## Deuteron Magnetic Form Factor Measurements of High Momentum Transfer

R. G. Arnold, D. Benton, P. Bosted, L. Clogher, G. DeChambrier, A. T. Katramatou, J. Lambert,<sup>(a)</sup>  
A. Lung, G. G. Petratos, A. Rahbar, S. E. Rock, and Z. M. Szalata  
*The American University, Washington, D.C. 20016*

R. A. Gearhart  
*Stanford Linear Accelerator Center, Stanford University, Stanford, California 94305*

B. Debebe, M. Frodyma, R. S. Hicks, A. Hotta,<sup>(b)</sup> and G. A. Peterson  
*University of Massachusetts, Amherst, Massachusetts 01003*

J. Alster and J. Lichtenstadt  
*Tel Aviv University, Tel Aviv 69978, Israel*

and

F. Dietrich and K. van Bibber  
*Lawrence Livermore National Laboratory, Livermore, California 94550*  
(Received 29 December 1986)

The deuteron magnetic form factor  $B(Q^2)$  has been measured at momentum transfers  $Q^2=1.21, 1.49, 1.61, 1.74, 1.98, 2.23, 2.48, 2.53,$  and  $2.77$   $(\text{GeV}/c)^2$  at the Stanford Linear Accelerator Center by detection of electrons backscattered at  $180^\circ$  in coincidence with recoiling deuterons at  $0^\circ$ . The data for  $B(Q^2)$  are found to decrease rapidly from  $Q^2=1.2$  to  $2$   $(\text{GeV}/c)^2$ , then rise to a secondary maximum around  $Q^2=2.5$   $(\text{GeV}/c)^2$ , in qualitative agreement with impulse-approximation calculations.

PACS numbers: 25.30.Bf, 25.10.+s, 27.10.+h

The elastic electromagnetic form factors of the deuteron at high momentum transfer have long been of interest for the information they contain on the short-range nucleon-nucleon interaction and the transition from nucleon to quark degrees of freedom. Models<sup>1</sup> based on the impulse approximation predict a minimum in the magnetic form factor somewhere between four-momentum transfers  $Q^2=1.5$  and  $2.5$   $(\text{GeV}/c)^2$ . Predictions for the diffractive shape of the magnetic form factor are sensitive to the high-momentum components in the deuteron wave function,<sup>2,3</sup> choice of nucleon form factors,<sup>4</sup> isobar contributions,<sup>5</sup> the contributions of isoscalar meson-exchange currents,<sup>5,6</sup> relativistic effects,<sup>2,7-10</sup> and the role of six-quark clusters.<sup>7,8,11-13</sup> Perturbative QCD predicts<sup>7,14</sup> a smooth falloff of the cross section, with no diffractive feature. To provide new information that will help distinguish between the various models, we have measured the deuteron magnetic form factor from  $Q^2=1.21$  to  $2.77$   $(\text{GeV}/c)^2$ , more than doubling the range in  $Q^2$  of the available data.

The cross section for elastic electron scattering from the deuteron can be written as

$$d\sigma/d\Omega = \alpha^2 E_{el}'/4E^3 \sin^4(\frac{1}{2}\theta) \\ \times [A(Q^2)\cos^2(\frac{1}{2}\theta) + B(Q^2)\sin^2(\frac{1}{2}\theta)],$$

where  $E$  and  $E_{el}'$  are the incident- and scattered-electron energies, and  $\theta$  is the electron scattering angle. The structure function  $A(Q^2)$  is a combination of the charge,

quadrupole, and magnetic form factors, and has previously<sup>15</sup> been measured out to  $Q^2=4$   $(\text{GeV}/c)^2$ . The magnetic form factor  $B(Q^2)$  has been measured<sup>16</sup> out to  $Q^2=1.3$   $(\text{GeV}/c)^2$ . The predictions of most calculations and extrapolation of previous data show  $B(Q^2)$  becoming more than two orders of magnitude smaller than  $A(Q^2)$  at higher  $Q^2$ . For this reason we decided to make our measurements close to  $180^\circ$ , where the contribution from  $A(Q^2)$  is small. The anticipated low counting rates dictated the use of thick targets, high beam intensity, and a large solid angle. The resulting loss in energy resolution made it necessary to detect the recoiling deuterons at  $0^\circ$  to separate elastic and inelastic scattering.

Figure 1 shows a layout of the spectrometer system<sup>17</sup> that was built in end station A at the Stanford Linear Accelerator Center. Electrons from the new nuclear-physics injector were accelerated to between 0.7 to 1.3 GeV, with an energy spread limited by slits to  $\pm 0.4\%$ . The maximum beam intensity was  $5 \times 10^{11}$  electrons per 1.6- $\mu\text{sec}$ -long pulse, at a maximum repetition rate of 150 Hz. The electron beams were transported through dipole magnets B1, B2, and B3 to the target, then deflected by dipole B5 into a heavily shielded dump located in the end station. Both dipole B2 and the dump were remotely movable.

The electrons scattered near  $180^\circ$  were focused by quadrupoles Q1-Q3 and momentum analyzed by dipoles B3 and B4. The electron spectrometer had a solid angle

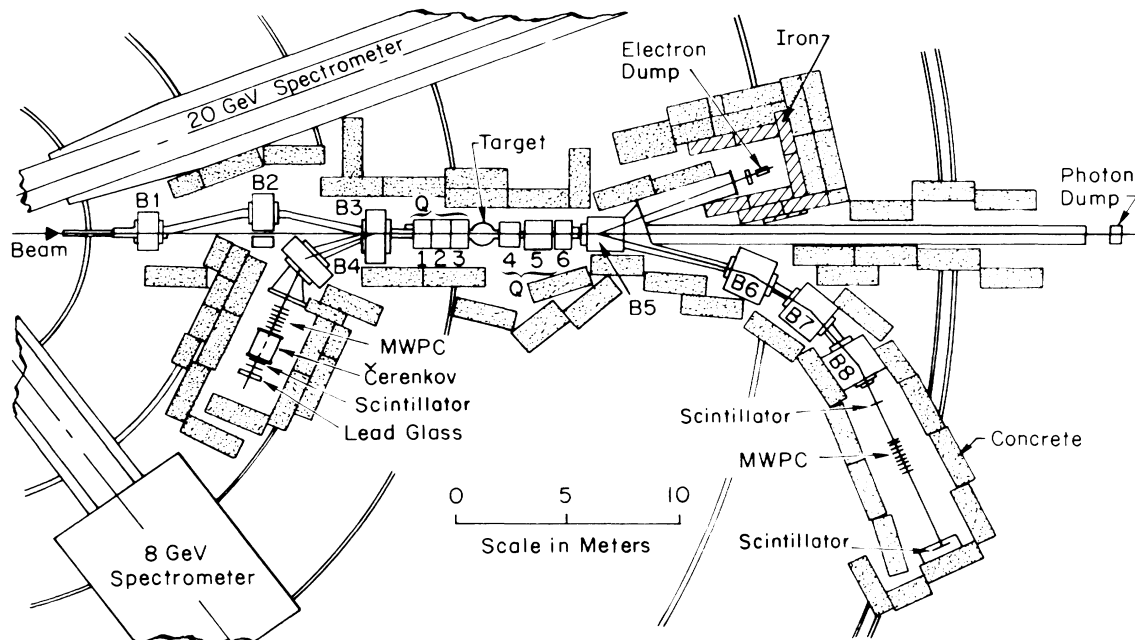


FIG. 1. Experimental layout in end station A at SLAC.

of 20 msr for a 20-cm-long target and a momentum acceptance of  $\pm 4\%$ . The angular and momentum resolutions were typically  $\pm 10$  mr and  $\pm 0.5\%$ , respectively. The electron momenta  $E'_{el}$  for  $ed$  elastic scattering were from 0.41 to 0.54 GeV/c, while the recoil momenta  $P_{el}$  ranged from 1.1 to 1.9 GeV/c. The  $0^\circ$  recoil spectrometer used quadrupoles Q4–Q6 to focus and dipoles B5–B8 to momentum analyze the recoil nuclei. The momentum acceptance was  $\pm 2\%$  and solid angle was about 6 msr, large enough to match completely the electron-arm solid angle for elastic kinematics. The momentum resolution of the recoil spectrometer was  $\pm 0.5\%$ , and the angular resolution  $\pm 10$  mr. The entire beam transport system up to the detectors was under vacuum and was heavily shielded on all sides.

The target system contained liquid deuterium, liquid hydrogen, and empty cells of lengths 5, 10, 20, and 40 cm. The liquids were pressurized to 2 atm and pumped at high velocity through the cells to heat exchangers cooled to 21 K with liquid hydrogen. Beam-induced density changes were measured to be less than 1%.

Scattered particles were detected in the electron arm by a threshold gas Čerenkov counter filled with Freon-12 at atmospheric pressure and a forty-segment lead-glass shower counter of 15 radiation lengths. This detector package was  $> 98\%$  efficient for detecting electrons, while rejecting essentially all of the large flux of pions. The particle trajectories were measured with  $> 97\%$  efficiency with six planes of multiwire proportional chambers (MWPC). Two scintillator arrays provided fast timing.

Particles were identified in the  $0^\circ$  recoil spectrometer

by time of flight (TOF) between two scintillator arrays placed 7 m apart. Eight planes of MWPC were used to reconstruct particle tracks with an efficiency of  $> 98\%$ . The principal background was a large flux of protons from  $d(\gamma,p)n$ . Very clean proton-deuteron separation by TOF was achieved in all cases. Time of flight between the electron and recoil-arm scintillators was used to identify electron-recoil coincidences.

The optical properties of the spectrometers and their solid angles including radiative effects were evaluated with a Monte Carlo computer program<sup>18</sup> which simulated the entire system. The program traced particles from the target to the detectors using detailed field maps that were made of each magnet. The effects from ionization loss, multiple scattering, finite target length, detector resolutions, limiting apertures, and radiation by the electrons were taken into account. The predicted vertical focusing properties of the electron spectrometer were verified by our taking special data using a set of small apertures between the target and Q3. Elastic  $ep$  scattering, which has a clear elastic peak and a large cross section, was measured at each beam energy. The  $ep$  data were used to verify the predicted momentum acceptances and dispersions in each arm, to calibrate the field settings versus momentum, and to check the solid angles as calculated by the Monte Carlo program. Excellent agreement was found between cross sections measured with the electron arm only and those measured with requirement of an electron-proton coincidence. The results were found to be independent of the target length used, and in excellent agreement with previous  $ep$  elastic measurements<sup>19</sup> in the same  $Q^2$  range.

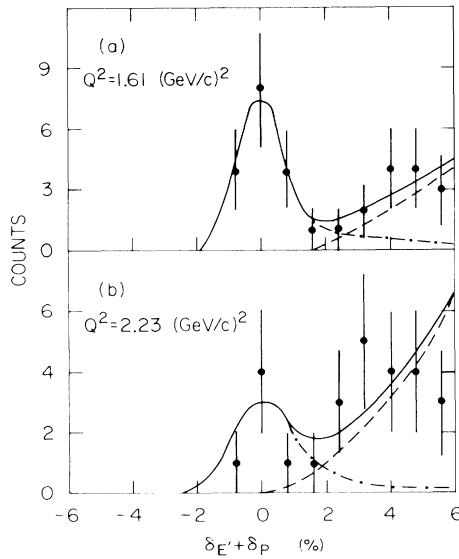


FIG. 2. Observed  $ed$  counts versus the sum of electron and deuteron missing momenta at two values of  $Q^2$ . The curves are normalized missing-momentum distributions from Monte Carlo calculations:  $ed$  elastic (dot-dashed); contributions from  $d(\gamma, \pi^0)d$  (dashed); sum (solid).

Data were taken in two running periods. The 20-cm-long target was used for all the data points except for  $Q^2=1.21$   $(\text{GeV}/c)^2$  (10-cm target) and  $Q^2=2.48$   $(\text{GeV}/c)^2$  (40-cm target). The electron-deuteron elastic signal was identified by use of TOF to identify  $ed$  coincidences, and kinematic cuts to isolate the  $ed$  elastic events from background. Plots of the number of observed  $ed$  coincidences versus total percentage missing momentum ( $\delta_{E'} + \delta_P$ ) for two values of  $Q^2$  are shown in Fig. 2. The missing momenta for the electrons and deuterons are defined as  $\delta_{E'} = (E'_{el} - E')/E'_{el}$  and  $\delta_P = (P_{el} - P)/P_{el}$ . Clear  $ed$  elastic peaks can be seen centered around  $\delta_{E'} + \delta_P = 0$ , as well as a substantial number of background events with large missing momenta. Comparison with Monte Carlo calculations and an extrapolation of measured cross sections<sup>20</sup> show the background counts to be consistent with contributions from  $d(\gamma, \pi^0)d$ , where one of the photons from the  $\pi^0$  decay produces a pair in the target to make the detected electron. The elastic counts were separated from background by a two-parameter fit of the Monte Carlo predictions for each of the processes (dot-dashed and dashed curves in Fig. 2). Even in the worst case [ $Q^2=2.23$   $(\text{GeV}/c)^2$ ] the background contribution to the elastic peak region was small.

After isolation of the  $ed$  elastic coincidences from the background events, corrections were made for dead time (2% to 5%), detector inefficiencies (6% to 12%), and absorption of deuterons in the target and recoil detectors (9% to 20%). End-cap contributions and random  $ed$

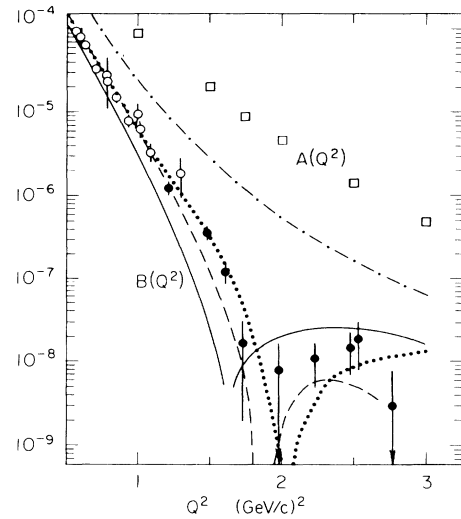


FIG. 3. Results for  $B(Q^2)$  from this experiment (solid circles) including both statistical and systematic errors, and previous data for  $B(Q^2)$  (open circles, Ref. 16) and  $A(Q^2)$  (squares, Ref. 15). The theoretical curves for  $B(Q^2)$  from Refs. 2, 7, or 9 (solid); Ref. 5 (dashed), Ref. 21 (dotted), Ref. 2 (indistinguishable from dotted curve) and Ref. 7 (dot-dashed) are described in the text.

coincidence rates were found to be negligible in most cases. A subtraction was made for the calculated contribution of  $A(Q^2)$  due to the finite angular acceptance of the electron spectrometer. This correction was largest at  $Q^2=1.98$   $(\text{GeV}/c)^2$ , where the ratio  $B(Q^2)/A(Q^2)$  becomes less than 0.002. The results for  $B(Q^2)$  are shown in Fig. 3 and listed in Table I. They correspond to extremely small cross sections, e.g.,  $d\sigma/d\Omega = (2.2 \pm 1.2) \times 10^{-41}$   $\text{cm}^2/\text{sr}$  at  $Q^2=2.23$   $(\text{GeV}/c)^2$ .

TABLE I. Values of four-momentum transfer  $Q^2$ , number of incident electrons  $N_{inc}$ , observed  $ed$  elastic counts  $N_{ed}$  (corrected for inefficiencies), calculated counts  $N_{A(Q^2)}$  from  $A(Q^2)$ , and results for  $B(Q^2)$ . The errors on both  $N_{ed}$  and  $B(Q^2)$  are dominated by the statistical error on the number of counts and the systematic uncertainty on the background separation.

$Q^2$ ( $\text{GeV}/c$ ) <sup>2</sup>	$10^{-18} N_{inc}$	$N_{ed}$	$N_{A(Q^2)}$	$10^8 B(Q^2)$
1.21	0.71	$44 \pm 8$	2.8	$126 \pm 24$
1.49	1.85	$44 \pm 8$	4.1	$36 \pm 7$
1.61	3.16	$27 \pm 7$	4.5	$12.2 \pm 3.6$
1.74	10.4	$17 \pm 8$	8.5	$1.7 \pm 1.5$
1.98	12.7	$8.2 \pm 4.6$	4.2	$0.8 \pm 0.9$
2.23	20.5	$9.9 \pm 4.0$	3.0	$1.1 \pm 0.6$
2.48	22.3	$16 \pm 8$	2.1	$1.5 \pm 0.8$
2.53	11.0	$6.0 \pm 3.0$	0.7	$1.9 \pm 1.1$
2.77	12.3	$1.3 \pm 1.3$	0.4	$0.3 \pm 0.5$

The new data for  $B(Q^2)$  join smoothly onto the previous data and show that the magnetic form factor of the deuteron continues to fall rapidly above  $Q^2=1.2$   $(\text{GeV}/c)^2$ . The ratio  $B(Q^2)/A(Q^2)$  also continues to decrease. A shallow diffraction minimum beginning around  $Q^2=1.8$   $(\text{GeV}/c)^2$  and a secondary maximum around  $Q^2=2.5$   $(\text{GeV}/c)^2$  can be seen. Comparison with a few representative predictions is made in Fig. 3. The results of a typical parton model<sup>7</sup> are shown as the dot-dashed curve. These models are expected to work best at high  $Q^2$ . In our  $Q^2$  range they predict a smooth falloff with no diffraction feature, and so can be ruled out by the present data. Much better qualitative agreement is found with impulse-approximation calculations. They predict a minimum in  $B(Q^2)$  somewhere between  $Q^2=1.5$  and  $2.0$   $(\text{GeV}/c)^2$ , with the height of the secondary maximum decreasing as the position of the minimum moves to higher  $Q^2$ . The principal uncertainty is in the choice of deuteron wave function. The results for the Paris wave function are shown as the solid line.<sup>2,7,9</sup> It can be seen that the minimum occurs at too low  $Q^2$  compared to the data. Agreement can be improved by modification of the impulse approximation in various ways. The dashed curve<sup>5</sup> includes isobar strengths adjusted to fit  $A(Q^2)$  and  $B(Q^2)$  at low  $Q^2$ , meson-exchange currents, and six-quark states. The main uncertainty in this calculation is the size of the  $\rho\pi\gamma$  coupling constant, which controls the size of the meson-exchange currents. A different way of treating exchange currents is in the Skyrme model,<sup>21</sup> which was used to predict the dotted curve in Fig. 3. Finally, still using the Paris wave function but now treating it relativistically, one calculation<sup>2</sup> produces a curve almost indistinguishable from the dotted one. We conclude that the nonrelativistic impulse approximation alone is not sufficient to describe our new data, but that the inclusion of other effects can bring this basic approach into reasonable agreement. Our new data for  $B(Q^2)$ , combined with previous data for  $A(Q^2)$  and nucleon-nucleon scattering data, will place severe constraints on the exact mixture of high-momentum components, nucleon form factors, meson-exchange currents, isobar admixtures, and treatments of relativistic effects and six-quark states used in the description of the short-range electromagnetic properties of the deuteron.

We would like to acknowledge the support of J. Davis,

B. Eisele, C. Hudspeth, J. Mark, J. Nicol, R. Miller, and the rest of the Stanford Linear Accelerator Center staff. This work was supported in part by the Department of Energy, Contracts No. DOE-AC03-76SF00515 (SLAC), No. W-7405-ENG-48 (LLNL), and No. DE-AC02-76ER-02853.A013 (University of Massachusetts) and National Science Foundation Grant No. PHY85-10549 (American University).

<sup>(a)</sup>Permanent address: Department of Physics, Georgetown University, Washington, D.C. 20057.

<sup>(b)</sup>Present address: School of Physics, Shizouka University, Shizouka 422, Japan.

<sup>1</sup>V. M. Muzafarov *et al.*, *Fiz. Elem. Chastits At. Yadra* **14**, 1112 (1983) [*Sov. J. Part. Nucl.* **14**, 467 (1983)], and references therein.

<sup>2</sup>R. S. Bhalero and S. A. Gurvitz, *Phys. Rev. C* **24**, 2273 (1981).

<sup>3</sup>R. G. Arnold, C. E. Carlson, and F. Gross, *Phys. Rev. C* **21**, 1426 (1980).

<sup>4</sup>I. I. Belyantsev *et al.*, *J. Phys. G*, **9**, 871 (1983).

<sup>5</sup>E. Lomon, P. Blunden, and P. Sitarski, in *Proceedings of the IUPAP International Nuclear Physics Conference, Harrogate, United Kingdom, August, 1986*, edited by G. C. Morrison (Institute of Physics, London, 1986), Vol. 1, p. 478.

<sup>6</sup>M. Gari and H. Hyuga, *Nucl. Phys.* **A264**, 409 (1976).

<sup>7</sup>M. Chemtob and S. Furui, *Nucl. Phys.* **A454**, 548 (1986).

<sup>8</sup>A. P. Kobushkin and V. P. Shelest, *Fiz. Elem. Chastits At. Yadra* **14**, 1146 (1983) [*Sov. J. Part. Nucl.* **14**, 483 (1983)].

<sup>9</sup>I. L. Grach and L. A. Kondratyuk, *Yad. Fiz.* **39**, 316 (1984) [*Sov. J. Nucl. Phys.* **39**, 198 (1984)].

<sup>10</sup>M. S. Zuilhof and J. A. Tjon, *Phys. Rev. C* **24**, 736 (1981).

<sup>11</sup>T. S. Cheng and L. Kisslinger, Carnegie Mellon Report No. PRINT-86-0898, 1986 (to be published).

<sup>12</sup>S. Takeuchi and K. Yazaki, *Nucl. Phys.* **A438**, 605 (1985).

<sup>13</sup>N. Honzawa *et al.*, *Prog. Theor. Phys.* **73**, 1502 (1985).

<sup>14</sup>S. Brodsky and B. Chertok, *Phys. Rev. D* **14**, 3003 (1976).

<sup>15</sup>R. Arnold *et al.*, *Phys. Rev. Lett.* **35**, 776 (1975).

<sup>16</sup>S. Auffret *et al.*, *Phys. Rev. Lett.* **54**, 649 (1985); R. Cramer *et al.*, *Z. Phys. C* **29**, 513 (1985).

<sup>17</sup>G. G. Petratos, SLAC Report No. NPAS-TN-86-7, 1986 (to be published).

<sup>18</sup>A. Katramatou, SLAC Report No. NPAS-TN-86-8, 1986 (to be published).

<sup>19</sup>L. E. Price *et al.*, *Phys. Rev. D* **4**, 45 (1971).

<sup>20</sup>A. Imanishi *et al.*, *Phys. Rev. Lett.* **54**, 23 (1985).

<sup>21</sup>E. M. Nyman and D. O. Riska, *Phys. Rev. Lett.* **57**, 3007 (1986).